AGU PUBLICATIONS

JGR

Journal of Geophysical Research: Atmospheres

RESEARCH ARTICLE
10.1002/2013JD021213

Key Points:
- Optically weighted growth factor was derived from light extinction measurements
- GF is found to be a more robust measure of hygroscopic growth than *f*(RH)
- Nonsea-salt marine supermicron aerosol components are moderately hygroscopic

Supporting Information:
- Readme
- Figure S1
- Figure S2
- Figure S3
- Figure S4
- Figure S5
- Figure S6
- Figure S7
- Figure S8
- Figure S9
- Figure S10
- Figure S11

Correspondence to:
C. D. Cappa,
cdcappa@ucdavis.edu

Citation:
Zhang, X., P. Massoli, P. K. Quinn, T. S. Bates, and C. D. Cappa (2014), Hygroscopic growth of submicron and supermicron aerosols in the marine boundary layer, *J. Geophys. Res. Atmos.*, *119*, 8384–8399, doi:10.1002/2013JD021213.

Received 19 NOV 2013
Accepted 5 JUN 2014
Accepted article online 10 JUN 2014
Published online 14 JUL 2014

Hygroscopic growth of submicron and supermicron aerosols in the marine boundary layer

Xiaolu Zhang[1], Paola Massoli[2], Patricia K. Quinn[3], Timothy S. Bates[3,4], and Christopher D. Cappa[1]

[1]Department of Civil and Environmental Engineering, University of California, Davis, California, USA, [2]Aerodyne Research, Billerica, Massachusetts, United States, [3]Pacific Marine Environmental Laboratory, National Oceanic and Atmospheric Administration, Seattle, Washington, USA, [4]Now at Joint Institute for the Study of the Atmosphere and Ocean, University of Washington, Seattle, Washington, USA

Abstract We investigate hygroscopic growth of marine aerosols from three research cruises: Texas Air Quality Study-Gulf of Mexico Atmospheric Composition and Climate Study (TexAQS-GoMACCS) 2006, International Chemistry Experiment in the Arctic Lower Troposphere (ICEALOT) 2008, and California Research at the Nexus of Air Quality and Climate Change (CalNex) 2010. Particle hygroscopic growth was characterized by measuring the effect of water uptake under subsaturated conditions on the aerosol light extinction at 532 nm. Mie theory calculations were utilized to convert the observed optical growth factors (f_{ext}(RH)) into physical growth factors (GF) at 85% RH. GF is found to be a more robust measure of aerosol hygroscopic growth than f_{ext}(RH), which can be biased by changes in aerosol dry size. Consistent with previous observations, the overall GF(85%) for submicron aerosol depended on the fraction of organics. The submicron GF_{OM}(85%) specifically was found to range from 1.0 to 1.3 for all three campaigns. A robust positive linear dependence of the overall supermicron GF(85%) on the mass fraction of sea salt was observed. During TexAQS, two types of dust particles with distinct hygroscopic properties were identified in the supermicron mode; one that originated from the Sahara desert was moderately hygroscopic (GF_{dust}(85%) = ~1.4) and the other from continental sources was nearly hydrophobic. The GF(85%) of supermicron organics was estimated through hygroscopicity closure calculations. Supermicron organics that originated from marine sources were found to be substantially more hygroscopic than those from continental sources, with the latter having a GF(85%) similar to that of the submicron organics. This study demonstrates the potential of using aerosol optical measurements to retrieve hygroscopic growth factor and underlines the importance and need for future investigations on the hygroscopic properties of marine supermicron aerosols.

1. Introduction

Atmospheric aerosols affect Earth's radiative balance and climate directly through absorption and scattering of the incoming solar radiation and indirectly through modification of cloud properties [*Intergovernmental Panel on Climate Change*, 2007]. Hygroscopicity, which characterizes the ability of aerosols to take up water under subsaturated and supersaturated conditions, is a key parameter determining both the direct and indirect climate effects of aerosols. It is well known that the hygroscopic growth of soluble particles can be described by the Köhler theory [*Köhler*, 1921, 1936]. Nonetheless, it remains challenging to characterize the hygroscopic behaviors of the dynamic and complex atmospheric aerosol consisting of particles with a wide range of sizes and chemical composition. As such, it is not surprising that representations of aerosol hygroscopicity in current atmospheric chemistry, and climate models are highly simplified and uncertain [*Malm and Kreidenweis*, 1997; *Kinne et al.*, 2003; *Ghan et al.*, 2012]. Numerous efforts have been made to develop instruments and techniques that quantitatively determine atmospheric aerosol hygroscopicity in situ. These measurements combined with chemical speciation data provide direct observational constraints for improving model parameterizations of hygroscopic properties of atmospheric aerosols.

Hygroscopic growth under subsaturated condition can be described by the hygroscopic growth factor (GF), which is the ratio of equilibrium particle diameters (D_p) under dry and wet conditions:

$$\mathrm{GF(RH)} = \frac{D_{p,\mathrm{wet}}}{D_{p,\mathrm{dry}}} \quad (1)$$

In principle, GF can be derived from the detected changes in particle size, mass, or optical properties due to water uptake. Instruments for direct quantification of GF based on particle size measurements (direct or inferred

from light scattering), such as the Hygroscopicity Tandem Differential Mobility Analyzer (H-TDMA) [*Liu et al.*, 1978; *Rader and McMurry*, 1986] and the Differential Aerosol Sizing and Hygroscopicity Spectrometer Probe (DASH-SP) [*Hersey et al.*, 2009; *Sorooshian et al.*, 2008], have been deployed to determine subsaturated aerosol hygroscopic growth in a wide range of atmospheric environments. The link between submicron aerosol GF and chemical composition has been extensively studied [e.g., *Gysel et al.*, 2007; *Hersey et al.*, 2009; *Cerully et al.*, 2011; *Duplissy et al.*, 2011; *Stock et al.*, 2011; *Hersey et al.*, 2013; *Wu et al.*, 2013]. However, an important limitation of these techniques is that they are only applicable for small particles due to the restriction of particle size range by the Differential Mobility Analyzers (typically dry diameter < 300 nm for high relative humidity (RH) conditions). GF measurements of larger (e.g., coarse) particles require different techniques and are sparse in the literature [*Hitzenberger et al.*, 1997; *Hegg et al.*, 2006, 2008; *Stock et al.*, 2011].

Besides these techniques for direct measurement of GF, an optical approach that involves measurements of aerosol light extinction (or scattering) at dry and humidified conditions has also been utilized to characterize the impact of particle water uptake on optical properties [e.g., *McInnes et al.*, 1998]. The ratio between the extinction coefficients (b_{ext}) of the humidified and dried aerosols is defined as the optical growth factor, often referred to as f_{ext}(RH):

$$f_{ext}(\mathrm{RH}) = \frac{b_{ext,wet}}{b_{ext,dry}} \tag{2}$$

Since this optical approach does not require the direct measurement of wet particle diameter, it is in principle applicable for a wider range of particle sizes. Some studies have further converted f_{ext}(RH) to an approximately RH-independent single-parameter, γ_{ext}, which represents a presumed power law continuous growth of aerosol light extinction as the RH approaches 100% [*Gassó et al.*, 2000; *Quinn et al.*, 2005; *Kim et al.*, 2006; *Massoli et al.*, 2009]. f(RH) and γ_{ext} have been extensively characterized in field and laboratory studies in which the dependence of f(RH) and γ_{ext} on aerosol chemical composition have been investigated [*Carrico et al.*, 2003; *Malm and Day*, 2001; *Malm et al.*, 2003; *Quinn et al.*, 2005, 2006; *Wang et al.*, 2007; *Ziemba et al.*, 2013; *Zhang et al.*, 1994]. For example, f_{ext}(RH) and γ_{ext} were both found to exhibit a negative correlation with the mass fraction of particulate organic matter (POM) in submicron aerosols sampled during New England Air Quality Study (NEAQS) 2004 [*Quinn et al.*, 2006] and Texas Air Quality Study-Gulf of Mexico Atmospheric Composition and Climate Study (TexAQS-GoMACCS) 2006 [*Massoli et al.*, 2009], respectively.

In more recent studies, an optically weighted hygroscopic GF was retrieved from the measured f_{ext}(RH) for laboratory-generated aerosols [*Cappa et al.*, 2011; *Flores et al.*, 2012; *Prather et al.*, 2013]. This inverse approach, based on Mie theory under the assumption of spherical particles, takes into account the changes in both the physical size and the refractive index of aerosols due to water uptake. Compared to f_{ext}(RH) and γ_{ext}, the optically weighted GF is more straightforwardly linked to model parameterizations. It should be noted that almost all these previous applications of the optical hygroscopic growth measurement techniques have only investigated submicron particles, although the method does allow for the extension to larger size ranges.

In this work, f_{ext}(RH) measurements and complementary aerosol chemical composition data for PM_1 and PM_{10} aerosols from three research cruises are analyzed. The algorithm developed by *Cappa et al.* [2011] has been used for the first time to retrieve hygroscopic GF from f_{ext}(RH) for both submicron and supermicron aerosols collected in coastal and marine boundary layer atmospheres during these cruise campaigns. Variations in GF for a relatively wide range of chemical composition sampled in different regions are examined. In particular, the results on the hygroscopic properties of supermicron aerosols, for which in situ observational studies are scarce and in need, are highlighted. Results from this study will be a valuable addition to the understanding of hygroscopicity of marine aerosols, especially in the supermicron range, and provide observational constraints for the representation of marine aerosol hygroscopic growth in climate models.

2. Methods

2.1. Field Campaigns

The data sets analyzed in this study were collected from three NOAA sponsored research cruises (data available for download at http://saga.pmel.noaa.gov/data/). A map that shows the cruise tracks is presented in Figure S1 in the supporting information. The TexAQS-GoMACCS (Texas Air Quality Study-Gulf of Mexico Atmospheric Composition and Climate Study) took place during the period of 27 July to 11 September 2006 near the Texas

Gulf coastal region, with the goals of better understanding the sources, atmospheric processes, and radiative properties of aerosols over the Gulf of Mexico [*Bates et al*., 2008]. Aerosol optical and chemical composition measurements were made on board the NOAA R/V *Ronald H. Brown*. The ICEALOT (International Chemistry Experiment in the Arctic Lower Troposphere) campaign was conducted in the spring of 2008 (19 March to 24 April 2008) to characterize the sources and distribution of gas and aerosol phase pollutants within the Arctic marine boundary layer. Measurements used in this study were made aboard the Woods Hole Oceanographic Institute (WHOI) R/V *Knorr*, most of the time cruising in an ice-free region of the Arctic during the campaign [*Frossard et al*., 2011]. The CalNex (California Research at the Nexus of Air Quality and Climate Change) campaign, conducted in the spring-summer time of 2010, was a multiplatform field study that aimed to understand the interactions between regional air quality and climate change issues [*Ryerson et al*., 2013]. As part of CalNex, aerosol measurements were made aboard the WHOI R/V *Atlantis* along the California coast from mid-May to mid-June 2010. A large fraction of the data were collected near the Los Angeles coastal region sampling air masses influenced by urban and ship emissions.

During these cruises, aerosol particles were sampled ~18 m above the sea surface through a ~5 m tall inlet mast. The inlet nozzle was designed to rotate with wind to maintain a nominally isokinetic flow and to minimize the loss of supermicron particles. The lower part of the mast was moderately heated so that the sampled air was maintained at $<$25% relative humidity (RH) during ICEALOT and $<$60% RH during TexAQS and CalNex. The sampled aerosols were directed to a variety of instruments and impactors via 1.9 cm diameter stainless steel or conductive polyethylene tubes that extended into the heated zone of the inlet. Further details about the sampling mast were provided by *Bates et al*. [2002].

2.2. Measurements

2.2.1. CRD-AES Light Extinction and f_{ext}(RH)

Aerosol extinction (b_{ext}) and subsaturated hygroscopic growth f_{ext}(RH) measurements were made with a cavity ring-down aerosol extinction spectrometer (CRD-AES) similar to that described in *Langridge et al*. [2011]. An automated valve was placed upstream of the CRD-AES to switch the sample flow between two Berner-type impactors [*Berner et al*., 1979] to select either sub-10 μm (PM_{10}) or sub-1 μm particles (PM_1). Extinction due to supermicron particles (PM_{super}) was determined by taking the difference between the observed $b_{ext}(PM_{10})$ and the average $b_{ext}(PM_1)$ as measured just prior to and just after the PM_{10} measurement. The CRD-AES used during the three campaigns had four channels operating at 532 nm, one channel at 355 nm, and one at 1064 nm. The effect of water uptake on the light extinction was measured by operating one of the 532 nm channels under dry RH ($<$30%) with a Nafion diffusion dryer (Perma Pure) and two of the 532 nm channels at an elevated RH (i.e., 75% and 85%) with custom-built humidifiers. The RHs in the cavity were monitored using calibrated RH and temperature probes (Rotronic Inc.). The fourth 532 nm channel was dried and filtered to determine the interference from gas-phase species to the observed signal. The particle loss in the Nafion dryer was estimated to be ~10%. The accuracy of the RH measurement is ±2%. Not counting particle losses, the uncertainty is estimated to be within ±3% for the PM_1 and PM_{10} CRD extinction measurements. The uncertainty in the derived supermicron particle extinction depends on the PM_{10}/PM_1 extinction ratio. As this ratio increases, the uncertainty in supermicron extinction decreases. For a PM_{10}/PM_1 extinction ratio $>$1.25, the propagated uncertainty in supermicron extinction is $<$20%.

The f_{ext}(RH) was calculated using the measured 532 nm aerosol extinction coefficients (b_{ext}) at dry (RH $<$ 30%) and humidified (RH = 75% ~ 90%) conditions (equation (2)). Because the RHs for the humidified cells were not actively controlled, and thus exhibited some fluctuations in time, a dimensionless, RH-independent parameter, γ_{ext}, was obtained by combining the three CRD 532 nm extinction measurements at dry and elevated RH:

$$\gamma_{ext}\frac{\log\left(f_{ext}(\mathrm{RH})\right)}{\log\left[\left(100-\mathrm{RH}_{dry}\right)/\left(100-\mathrm{RH}\right)\right]} \tag{3}$$

where in our study RH_{dry} is 25%. Using equation (3), f_{ext}(RH) at exactly 85% RH was determined to facilitate comparison between different time periods and to further allow for retrieval of the optically weighted GF at 85% RH (detailed in section 3). The uncertainty of the derived f_{ext}(85%) for submicron particles is largely determined by the accuracy of the RH measurement. A ± 2% error in RH measurement translates to an uncertainty of ±7% in f_{ext}(85%) for a typical γ_{ext} value of 0.5.

It is possible that particle losses between the humidifier and humidified channels were increased relative to the dry channel due to the increase in particle aerodynamic diameter with water uptake, with such an effect being most important for the supermicron particles. Loss of semivolatile aerosol components (i.e., ammonium nitrate) upon inlet heating during TexAQS and CalNex may have also occurred. Such losses would lead to a low bias in the observed f_{ext}(RH) and derived GF, and thus, the reported GFs are lower limits. However, as will be shown below, the magnitude of the derived GFs from CalNex and TexAQS when the sea-salt fraction is large suggests that the supermicron GFs are not substantially underestimated. The f_{ext}(RH) data for supermicron particles from ICEALOT were discarded due to additional biases introduced by the different conditions under which the measurements were made. The ambient temperature in ICEALOT (often near or below the freezing point) was substantially lower than the indoor temperature, while for both TexAQS and CalNex the indoor temperature was much more similar to the outdoor temperature. As a result, the sampled particles were effectively dried during ICEALOT from warming, while the sampling line RH during TexAQS and CalNex was close to ambient RH. When sampling PM_{10}, we suspect that the residence time in the CRD-AES humidifier during ICEALOT was insufficient to allow for sufficient water uptake given the large absolute amount of water required and the small starting RH. For PM_1, much less water needed to be transferred to the particles, and it is believed that the particles were able to reach equilibrium. Comparison of the f_{ext}(RH) data for PM_1 to similar data collected during ICEALOT for particle scattering (i.e., f_{sca}(RH)) indicates that there is no substantial bias in the submicron f_{ext}(RH) observations.

2.2.2. Aerosol Chemical Composition

Time series concentrations of nonrefractory (NR) submicron aerosol NH_4^+, NO_3^-, SO_4^{2-}, and particulate organic matter (POM) were determined with a Quadrupole Aerosol Mass Spectrometer (Q-AMS) (Aerodyne Research Inc.) [*Jayne et al*., 2000; *Allan et al*., 2003] sampling downstream of a PM_1 impactor. The collection efficiency of the AMS varied from 0.54 to 1, dependent upon aerosol chemical composition, and therefore was assigned to each 5 min sample based on AMS ammonium to sulfate molar ratio. The overall measurement uncertainty was estimated to be 20%. Further details about the Q-AMS operation and calibration are reported by *Bates et al*. [2008].

PM_1 and PM_{10} particles (50% aerodynamic cutoff diameters) were collected using multijet cascade impactors [*Berner et al*., 1979] with sampling times ranging from 2 to 23 h. The total number of impactor samples was 107, 52, and 49 for TexAQS, ICEALOT, and CalNex, respectively. The collected particles were analyzed offline for organic carbon (OC), elemental carbon (EC), trace elements, inorganic ions, and particle mass [*Bates et al*., 2008]. Two-stage and one-stage impactors were used to collect PM_1 and PM_{10} particles for OC/EC analysis, respectively. A denuder was deployed upstream of the submicron impactor to minimize interference from gas-phase organic species. OC and EC concentrations were determined with a Sunset Laboratory OC/EC analyzer following the *National Institute for Occupational Safety and Health* (NIOSH) [1996] protocol. The difference in concentrations between the two impactors was attributed to supermicron particles with aerodynamic diameter between 1 and 10 μm. Submicron organic aerosol mass (OM) was determined using the Q-AMS measurements. Supermicron OM was determined by multiplying the impactor OC concentration by a constant factor of 2.0 [*Turpin and Lim*, 2001; *Bates et al*., 2008]. The uncertainty of the impactor OC was estimated to be ±13% for OC and ±33% for supermicron OM (including ±31% uncertainty associated with the OM/OC ratio) [*Bates et al*., 2008]. Seven-stage impactors were used for inorganic ion analysis. The four smaller stages were combined to get submicron concentrations, and the three larger stages were combined to get supermicron concentrations. Cation (Na^+, NH_4^+, K^+, Mg^{2+}, and Ca^{2+}) and anion (Cl^-, NO_3^-, and SO_4^{2-}) concentrations were quantified using ion chromatography. Measurement uncertainty of the water-soluble ions was estimated to be ±8.5%. Sea-salt (SS) aerosol mass concentration ($\mu g\, m^{-3}$) was calculated as follows:

$$[SS] = [Cl^-] + [Na^+] \times 1.47 \tag{4}$$

Concentrations of trace elements (Na, Mg, Al, Si, P, Cl, K, Ca, Ti, V, Cr, Mn, Fe, Ni, Cu, Zn, Ba, As, and Pb) were determined using thin-film X-ray primary and secondary emission spectrometry [*Bates et al*., 2004]. The inorganic oxidized material (IOM) that was mainly composed of dust, and/or fly ash was constructed based on elemental data as follows:

$$[IOM] = 2.2[Al] + 2.49[Si] + 1.63[Ca] + 2.42[Fe] + 1.94[Ti] \tag{5}$$

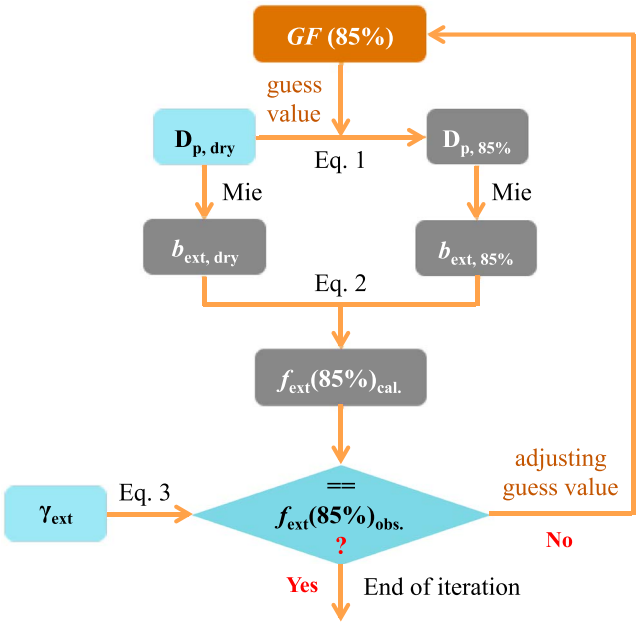

Figure 1. Schematic representation of the iterative algorithm for retrieving the hygroscopic growth factor (GF) at 85% RH from the f_{ext}(RH) measurement.

[*Malm et al.*, 1994]. The average overall uncertainty in the IOM mass was ±12% [*Bates et al.*, 2008]. In the following analysis and discussion, IOM is used as a surrogate of the dust component in submicron and supermicron particles.

2.2.3. Particle Number Size Distributions

Particle number size distributions in the diameter range of 20–800 nm Stokes diameter were measured by combining an "Aitken" Differential Mobility Particle Sizer (DMPS) (20–200 nm) and an "accumulation" DMPS (200–800 nm). The number size distributions of particles in the diameter range of 0.8–10 μm aerodynamic diameter were determined with an Aerodynamic Particle Sizer (APS). The two size distributions were merged by converting the APS data from aerodynamic diameters to Stokes diameters using particle densities calculated from measured aerosol chemical composition [*Bates et al.*, 2008]. The use of Stokes diameters over aerodynamic diameters is more appropriate for optical calculations as they represent the physical size of the particle under the assumption of spherical particles. The APS data adjustment also accounted for nonspherical particle shape [*Quinn et al.*, 2004]. The estimated uncertainty in the number concentration in each size bin was ±10%.

All of the size measurements were made at the inlet mast RH (<25% for ICEALOT and <60% for TexAQS and CalNex), whereas the "dry" optical property measurements were made at ~25% RH. If the particles retain water at 60% RH, the measured particle size would be overestimated relative to the optical property measurements. This would influence the ability to obtain absolute optical closure but has only a small influence on the conversion of f_{ext}(RH) to GF(85%), as illustrated through sensitivity tests shown in Figure S2.

3. Derivation of Hygroscopic GF

Following *Cappa et al.* [2011], an iterative algorithm, illustrated in Figure 1, was applied to retrieve GF at 85% RH using measured f_{ext}(85%) and dry particle size distribution for both submicron and supermicron data sets. Specifically, $b_{ext,532nm}$ values were calculated using Mie theory for both the dry particle size distribution and for a humidified (at 85% RH) particle size distribution [*Bohren and Huffman*, 1983]. The ratio between the diameters of the humidified particles and the dried particles correspond to GF(85%). The value of GF(85%) that corresponds to the observed f_{ext}(85%) was determined by increasing the GF(85%) from some initial guess value (typically GF = 1.0) in steps of 0.005 until the calculated f_{ext}(85%) agreed with the observed f_{ext} (85%) to within ±1%. The algorithm returns a null value for GF if the derived GF(85%) was unrealistically high (i.e., GF > 2.1). This was done separately for submicron and supermicron particles to determine values of GF_{sub} and GF_{super} at 85% RH, respectively. The temporal resolution of the retrieved GF(85%) is 10 min, based on the alternating sampling of PM_1 and PM_{10}. GF_{super}(85%) data were averaged to the impactor sampling periods (2–23 h) for further analysis. There is generally good agreement between the observed and calculated $b_{ext,532nm}$ for both submicron and supermicron particles (Figure S3), which suggests that the assumption of spherical particles in the Mie calculations is reasonable.

Values of several parameters used in this process need to be estimated prior to the GF derivation. For instance, the real part (n) of the dry particle refractive index (RI_{dry}) was assumed to be 1.50 based on measured aerosol chemical composition. The imaginary part (k) of RI_{dry} was set to scale with the black carbon (BC)

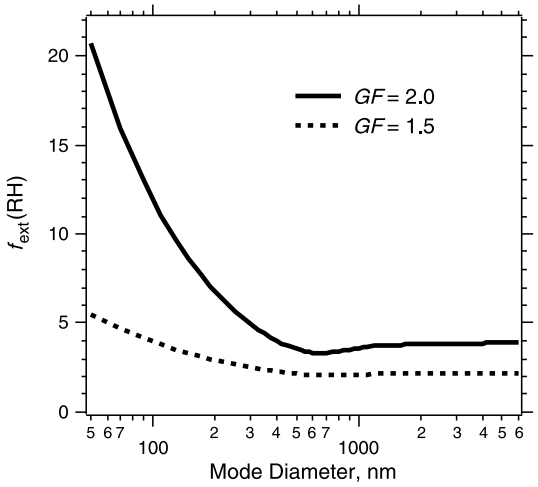

Figure 2. Variations in f_{ext}(RH) at 532 nm as a function of dry particle diameter (nm) for a constant growth factor of 1.5 or 2.0. f_{ext}(RH) is calculated based on Mie theory for lognormally distributed particles ($\sigma = 1.5$).

concentrations inferred from measured light absorption at 532 nm using a photoacoustic spectrometer, under the assumption that organics are nonabsorbing at 532 nm [*Lambe et al.*, 2013]. The wet particle refractive index (RI_{wet}) was determined using volume mixing rules assuming $RI_{water} = 1.33$. A particle Stokes diameter of 684.2 nm ($D_{p,cut}$) was used to separate submicron and supermicron dry particle number size distributions. The use of 684.2 nm, as opposed to 1 μm, is appropriate since the cutoff size of the impactors was aerodynamic diameter and the particle density was most likely >1 g cm^{-3}. This particular value was determined by minimizing the difference between calculated and measured dry particle $b_{ext,532nm}$ for both submicron and supermicron particles, which was generally within 15%. The model also assumes that the particle chemical composition is size independent within a given mode (submicron versus supermicron) and that all particle components are internally well mixed. To estimate the uncertainty of the retrieved GF(85%) introduced by the various model assumptions and from the measurement uncertainties of f_{ext}(85%) (±7%) and particle number concentration (±10%), a series of sensitivity tests have been performed, the results from which are summarized in Figures S4 and S5. It was found that GF (85%) was relatively insensitive to the changes in RI and $D_{p,cut}$. For example, varying the $D_{p,cut}$ by 22% (equivalent to ±150 nm in Stokes diameter) only introduced on average 2.5% change in the calculated GF for either submicron or supermicron particles, although it does have a substantial impact on the calculated absolute $b_{ext,532nm}$. The estimated uncertainty in the overall submicron and supermicron GF(85%) resulting from measurement uncertainties associated with f_{ext}(85%) was ±4% and ±18%.

4. Results and Discussions

4.1. The f_{ext}(RH) and GF for Submicron and Supermicron Aerosols

The f_{ext}(RH) (and γ_{ext}) depends on both dry aerosol size and the water content of the particle, with only the latter being associated with particle hygroscopic properties. As shown in Figure 2, in the submicron size range smaller particles will theoretically exhibit much larger f_{ext}(RH) values for a given GF (in this case GF = 1.5 or 2.0). The sensitivity of f_{ext}(RH) to size is much reduced in the supermicron range. Therefore, in theory, f_{ext}(RH) values provide only an approximate measure of particle hygroscopic growth as they are subject to variations in the particle dry size distribution, especially for submicron particles. The example shown in Figure 2 uses lognormally distributed particles ($\sigma = 1.5$) to illustrate the point. A distribution of atmospheric aerosols will exhibit overall smaller sensitivities to variations in particle size, as is indicated by the general insensitivity in the derived GF(85%) values to small errors in particle size discussed above. However, in comparing between different campaigns, where the nature of the observed size distributions may be quite different, conversion of the observed f_{ext}(RH) values to equivalent optically weighted GF values should provide a more robust quantitative measure of hygroscopic growth since variations in dry particle size are inherently accounted for in the inversion process.

Normalized frequency distributions of f_{ext}(85%) and GF(85%) for the three campaigns are shown in Figures 3a and 3b, respectively. For submicron aerosols, f_{ext}(85%) and GF(85%) exhibited similar distribution patterns and were in general proportional to each other with a relatively constant campaign-average ratio between f_{ext}(85%) and GF(85%) that ranged from 1.91 to 2.03 (Table 1). For supermicron aerosols, the f_{ext}(85%) to GF(85%) ratio was also similar for TexAQS and CalNex (1.49 and 1.65, respectively), but the distributions of GF(85%) are much broader than f_{ext}(85%). The distinct ratio between f_{ext}(85%)

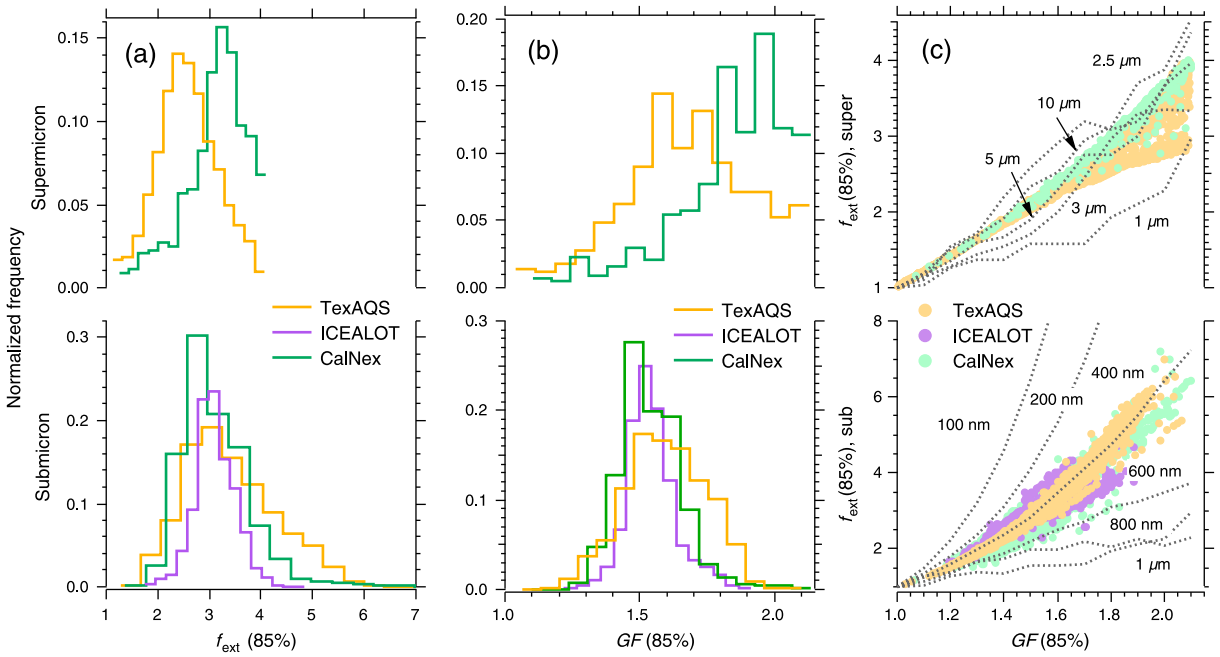

Figure 3. (a) Normalized frequency distributions of the measured submicron ($D_{p,dry} < 1$ μm) and supermicron (1 μm $< D_{p,dry} <$ 10 μm) particle f_{ext}(RH) at 85% RH for TexAQS, ICEALOT, and CalNex. (b) Same as Figure 3a but for the retrieved submicron and supermicron hygroscopic growth factor (GF) at 85% RH. (c) Scatterplots of submicron (bottom) and supermicron (top) f_{ext}(85%) versus the retrieved GF(85%) for the three campaigns. The dotted black lines are provided for reference and are the theoretical curves for the f_{ext}(85%) versus GF(85%) relationship, based on Mie calculation, for different monodisperse dry particle diameters in the submicron and supermicron size ranges. Supermicron f_{ext}(RH) and GF data from ICEALOT are not available for reasons discussed in section 2.2.

and GF(85%) for submicron and supermicron particles suggests that conversion from physical water uptake to the impact this water uptake has on particle light extinction should be treated differently for these two particle size ranges.

Further, although similar campaign-average ratio between f_{ext}(85%) and GF(85%) was obtained among the three campaigns (Table 1), Figure 3c shows the major role that the particle size effect plays in determining the dependence of f_{ext}(85%) on GF(85%), especially in the submicron size range. Consistent with theoretical calculations, when comparing hygroscopic behaviors of submicron particles with supermicron particles, f_{ext}(85%) is not a robust measure due to its high sensitivity to particle size (Figure 2). Taking data from TexAQS as an example, a comparison between submicron f_{ext}(85%) (mean ± 1σ: 3.22 ± 0.88) and supermicron f_{ext}(85%) (2.48 ± 0.58) would, by itself, suggest that submicron particles are much more hygroscopic than supermicron particles. However, the derived GF_{sub}(85%) (1.56 ± 0.15) was smaller than GF_{super}(85%) (1.64 ± 0.23), which indicates that submicron particles were actually less hygroscopic. Therefore, in the following analysis, we use the retrieved optically weighted GF as a measure of the overall aerosol hygroscopic growth. In all cases, the GFs correspond to 85% RH.

Table 1. Statistics of f_{ext}(RH) and GF at 85% RH for Submicron ($D_{p,dry} < 1$ μm) and Supermicron (1 μm $< D_{p,dry} <$ 10 μm) Particles During TexAQS, ICEALOT, and CalNex[a]

		Submicron ($D_{p,dry} < 1.0$ μm)			Supermicron (1.0 μm $< D_{p,dry} <$ 10 μm)		
		TexAQS 2006	ICEALOT 2008	CalNex 2010	TexAQS 2006	ICEALOT 2008	CalNex 2010
f_{ext} (85%)	Mean (±1σ)	3.22 ± 0.88	3.00 ± 0.38	2.91 ± 0.66	2.48 ± 0.58	N.A.	3.02 ± 0.60
	Range	1.08–6.98	1.65–4.72	1.16–7.19	1.02–3.97	N.A.	1.16–3.99
GF (85%)	Mean (±1σ)	1.56 ± 0.15	1.52 ± 0.09	1.51 ± 0.12	1.64 ± 0.23	N.A.	1.81 ± 0.21
	Range	1.03–2.07	1.20–1.89	1.07–2.10	1.00–2.10	N.A.	1.07–2.10
Mean f_{ext}(85%) to GF(85%) ratio		2.03	1.97	1.91	1.49	N.A.	1.65

[a]ICEALOT supermicron data have been excluded due to experimental complications (see text).

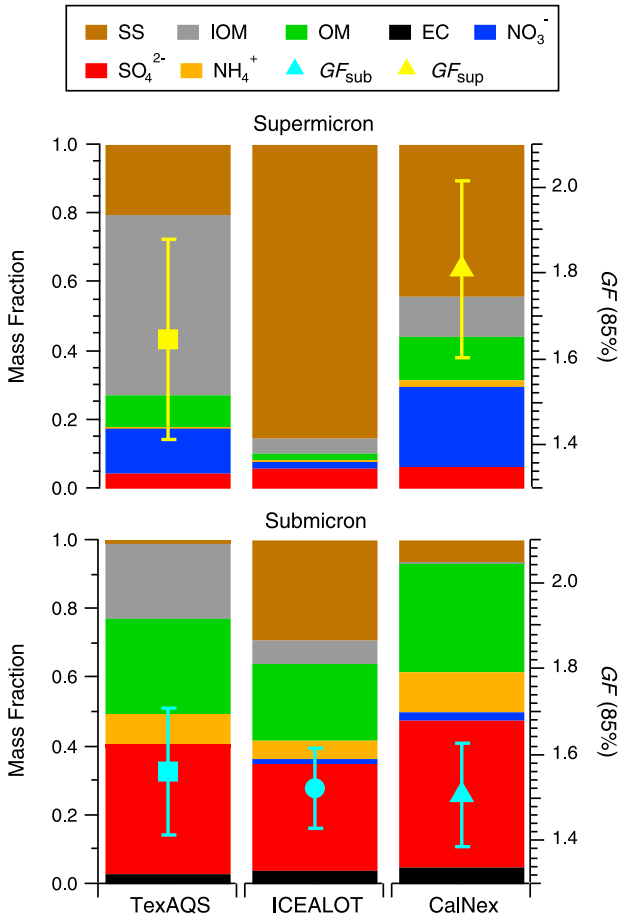

Figure 4. Campaign-average relative aerosol chemical composition (left axis, bars) and the mean (±1σ) hygroscopic growth factor (GF) at 85% RH (right axis, symbols) for dry submicron ($D_{p,dry} < 1$ μm) and supermicron (1 μm $< D_{p,dry} <$ 10 μm) particles. ICEALOT supermicron hygroscopicity data are not available for reasons discussed in section 2.2.

It is instructive to compare GF(85%) values among the campaigns and with those reported by previous studies. GF_{sub}(85%) showed similar distributions for the three campaigns, with ICEALOT GF_{sub}(85%) having a slightly narrower range, indicating less variability in the hygroscopic behaviors of submicron particles in the Arctic marine boundary layer than in urban coastal marine regions. This is consistent with the reasonably constant submicron particle composition observed during ICEALOT [*Frossard et al.*, 2011]. For CalNex, the mean GF_{sub} of 1.51 is comparable to the GF(85%) range of 1.45–1.72 for 150–200 nm particles measured with a DASH-SP off the coast of Central California during MASE-II [*Hersey et al.*, 2009]. The GF_{super}(85%) distributions were much broader and had larger mean values than GF_{sub}(85%) for both TexAQS and CalNex (Figure 3 and Table 1). Values of GF_{super} (85%) ~ 2.0 were observed in both regions. (For reference, the GF(85%) for NaCl, the primary inorganic component of sea spray, is ~2.1.) These results indicate that, in general, supermicron particles are more hygroscopic than submicron particles in these marine boundary layers. However, in contrast to the generally large GF_{super}(85%) distributions observed in this study, *Hegg et al.* [2006, 2008] reported descriptive hygroscopic GF (*DHGF*) values of only ~1.1–1.3 for 1–3.5 μm particles measured using an Aerosol Hydration Spectrometer on board the Center for Interdisciplinary Remotely-Piloted Aircraft Studies (CIRPAS) Twin Otter aircraft sampling at 30–500 m above sea level off the Monterey Bay, California. They typically observed lower values at 30 m altitude compared to 250 m and attributed the relatively low supermicron *DHGF* values to either inhibition of hygroscopic growth due to the presence of fatty acids or to the substantial presence of dust particles. In the next section, we examine in detail the relationship between GF and chemical composition for submicron and supermicron aerosols during the three campaigns.

4.2. Hygroscopic Growth and Chemical Composition

Figure 4 shows the average chemical composition of submicron and supermicron aerosols and the superimposed mean (±1σ) of GF_{sub}(85%) and GF_{super}(85%) for the three campaigns. OM and sulfate were the two largest components in submicron aerosols. Sea salt accounted for ~25% of the submicron aerosol mass in ICEALOT, much higher than the other two campaigns, which was likely a reflection of the remote sampling environment as well as the efficient sea spray aerosol production due to high wind speeds during ICEALOT. The IOM (dust) contribution to submicron aerosol mass was relatively high in TexAQS (~20%), largely due to the passage of dust storms (further discussed in section 4.3) during the sampling period. Sea salt (SS) and IOM are the dominant contributors in the supermicron particles. In particular, ICEALOT has the largest SS mass fraction (~85%), whereas TexAQS has the largest fraction of IOM (~50%).

Numerous studies have investigated the relationship between measured GF, f(RH), or γ and the aerosol chemical composition, although almost all focused exclusively on the submicron size range. Here the

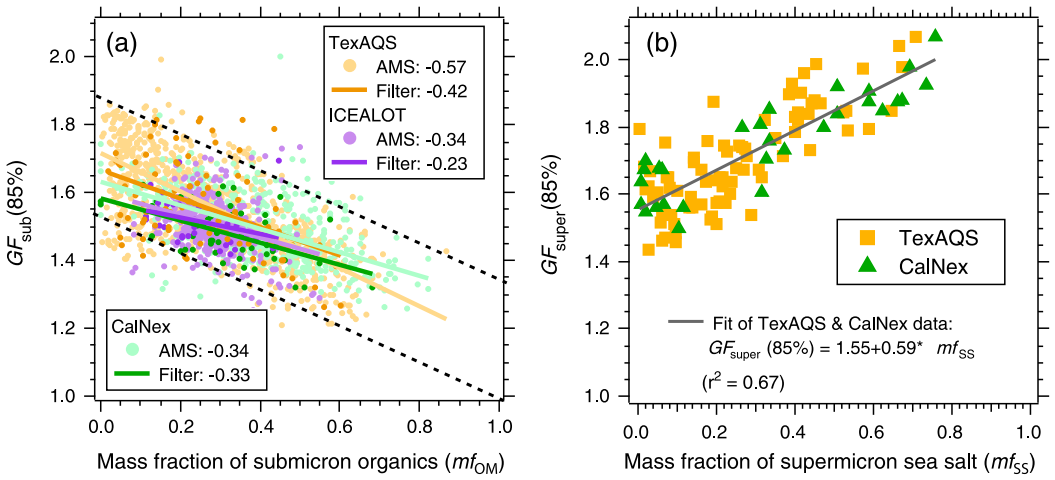

Figure 5. Scatterplots of (a) submicron aerosol growth factor (GF_{sub}) at 85% RH versus the mass fraction of submicron organic matter (mf_{OM}) from both the Q-AMS and the impactor measurements, and (b) supermicron aerosol growth factor (GF_{super}) at 85% RH versus the mass fraction of supermicron sea salt (mf_{SS}) from the impactor measurements. In Figure 5a, the slopes of the linear fits of the data for each category are listed. The dashed black lines are the 95% prediction bands for the linear fit of data from all the three campaigns.

relationship between both GF_{sub}(85%) and GF_{super}(85%) and the corresponding chemical composition (i.e., mass fractions of different chemical components measured with AMS and impactors) was examined. Considering first the submicron particles, a negative correlation was observed for all three campaigns between GF_{sub}(85%) and the mass fraction of organic matter (mf_{OM}) (Figure 5a), similar to the negative linear dependence of GF (determined with an H-TDMA) on the organic volume fraction for laboratory generated aerosols from β-pinene oxidation [*Virkkula et al.*, 1999], as well as the negative relationship found between γ_{ext} and the mass ratio of POM to POM + sulfate for ambient submicron aerosols during the Atmospheric Chemistry Experiment (ACE), the International Consortium for Atmospheric Research on Transport and Transformation (ICARTT), and TexAQS field studies [*Quinn et al.*, 2005; *Massoli et al.*, 2009]. Here mf_{OM} was determined for each of the three campaigns based on either the AMS NR-PM measurements, which exclude refractory BC, IOM, and sea salt, or the impactor measurements, which include the refractory materials.

Linear regressions of GF_{sub}(85%) versus mf_{OM} from the AMS NR-PM for individual campaigns gave very similar slopes for ICEALOT (−0.34) and CalNex (−0.34), whereas a much steeper slope was obtained for TexAQS data (−0.57). Based on all three campaigns' data, the average GF(85%) of submicron organics was estimated to be in the range of 1.0 and 1.33, as determined from the 95% prediction bands of the linear fit. Less negative slopes were obtained for TexAQS (−0.42) and ICEALOT (−0.23) when the mf_{OM} from the impactor measurements was used, likely because the impactor-derived mf_{OM} accounts for contributions from refractory materials (BC, dust, and sea salt) in addition to the NR components. The slopes determined using the impactor-derived and AMS-derived mf_{OM} from CalNex were very similar, most likely a reflection of contribution from submicron refractory materials being the smallest during this campaign (approximately 11% in total). Overall, these results highlight the important role that dust and SS play in modifying submicron aerosol hygroscopic properties in some remote and coastal marine atmospheres, as well as the challenge and the appreciable uncertainty associated with the simplified parameterization of the bulk composition dependence of the aerosol hygroscopic behavior.

(It should be noted that in a binary system where volume mixing rules apply, there should be a linear relationship between GF^3 and the volume fraction of one component, whereas the relationship between GF and mass fraction, or volume fraction, may not be strictly linear. In general, for a binary system, linear extrapolation of a GF versus mass fraction relationship will lead to an overestimation of both the more and less hygroscopic components, the extent of which will depend on the relative GFs of the two components and the range of mass fractions over which the data extend. Linear extrapolation in a multicomponent system adds an additional level of complexity that prohibits such simple analysis of whether extrapolation will lead to an over/underestimate of the "pure" component GFs. Here linear fits between the observed GF

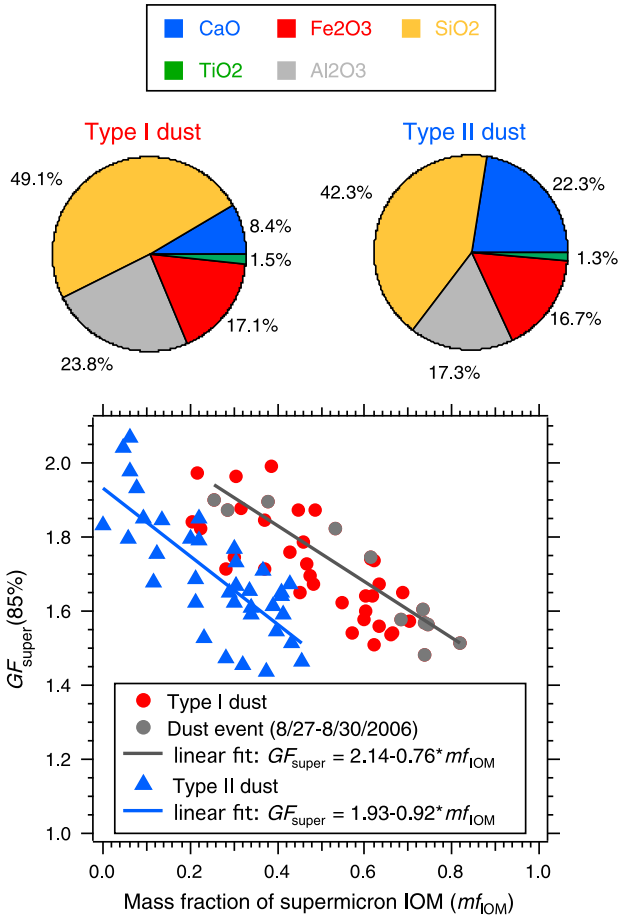

Figure 6. (top) Pie charts that illustrate the composition of the inorganic oxidized material (IOM) for the type I and type II dust. (bottom) Scatterplot of supermicron growth factor (GF_{super}) at 85% RH versus the mass fraction of supermicron IOM (mf_{IOM}) for the type I (red and gray circles) and type II dust (blue triangles). The data during the dust event from 27 to 30 August 2006 are highlighted as gray markers. The GF_{IOM}(85%) for type I and II dust were determined from the linear fits to GF_{super}(85%) versus mf_{IOM} extrapolated to $mf_{IOM} = 1$.

and mass fractions are used to be consistent with at least some of the literature and because, broadly speaking, the observed relationships are reasonably linear. Nonetheless, it should be kept in mind that the uncertainties in the derived pure-component GFs, such as that for the submicron organics above or some of the supermicron components below, may be underestimated from the regression statistics alone because the linear fit itself is only an approximation. Further discussion is provided in the supporting information (Figures S6 and S7).

Considering the supermicron particles, it is found that the relative fraction of sea salt (SS), determined from the impactor measurements, strongly controls the supermicron aerosol hygroscopic growth in TexAQS and CalNex, as suggested by the tight correlation between GF_{super}(85%) and the mass fraction of supermicron sea salt (mf_{SS}) (Figure 5b). A linear fit to the combined TexAQS and CalNex datasets yields a value of $GF_{super}(85\%) = 2.14$ when $mf_{SS} = 1$, consistent with the known hygroscopic growth of NaCl particle. This consistency suggests that particle losses between the humidifier and the extinction measurement cells did not substantially influence the measurements. It is noteworthy that the GF_{super}(85%) when $mf_{SS} = 0$ for these two campaigns is 1.55 (based on linear extrapolation), which suggests that the non-SS components are, on average, reasonably hygroscopic. This will be examined further for the TexAQS study in the next section.

4.3. Supermicron Particle Hygroscopic Growth: TexAQS Case Study

4.3.1. Hygroscopic Growth of Supermicron Dust

During TexAQS 2006, dust was a major component of the supermicron particle mass, especially during the period from 27 to 30August 2006 when a major dust event was encountered and impacted the air masses sampled at the ship [*Lack et al.*, 2009]. During this period, the total IOM mass loading increased up to 41.4 $\mu g\, m^{-3}$. The average IOM mass fractions were 53% and 59% for submicron and supermicron aerosols, respectively, which are 14.9 and 8.4 times higher than before the event. Hybrid Single-Particle Lagrangian Integrated Trajectory (HYSPLIT) back trajectories [*Draxler and Rolph*, 2013] (Figure 7) showed that the air masses during this particular event had originated from the Saharan region of North Africa and had been over the Atlantic Ocean for approximately a week before reaching the Gulf of Mexico, under the influence of the Azores High [*Bates et al.*, 2008]. The geochemical signatures (i.e., the mass ratio of Ca/Al, Fe/Al, and Si/Al) of the IOM component during the event quantitatively agreed with those of Saharan dust [*Formenti et al.*, 2003], which further confirmed the origin of the dust aerosols encountered during the event. Outside of this major dust event, there were some other periods where back trajectories showed a marine origin for the

air masses sampled, and where the IOM composition was very similar to that during the event, indicating that the dust aerosols during these mixed marine/dust periods also originated from the Sahara. The dust encountered during the major dust event and during the mixed marine/dust periods will be referred to as Type I dust. A second type of dust, referred to as Type II dust, that had a composition distinct from the Saharan dust and that had a different temporal profile was also encountered during TexAQS. The Type II dust was mainly sampled in September 2006, the last one third of the cruise, during which the source category was defined by northerly trajectories (Figure 7) and high radon concentrations. This suggests that the air masses with Type II dust that were intercepted by the ship had recently been over the North American continent (e.g., from the Ohio River Valley) [*Bates et al*., 2008; *Massoli et al*., 2009]. The Type II dust had a much higher fraction of CaO and lower fractions of SiO_2 and Al_2O_3 compared to Type I dust (Figure 6, top), consistent with the HYSPLIT back trajectories that indicated different source regions for the two dust types.

Interestingly, these two types of dust exhibited very different hygroscopic behaviors. Reasonably tight correlations between $GF_{super}(85\%)$ and the mass fraction of IOM, mf_{IOM}, in supermicron aerosols were observed for both Type I and Type II dust (Figure 6, bottom). From a linear fit to GF(85%) versus mf_{IOM} extrapolated to $mf_{IOM} = 1$, the GF for type I dust (the Saharan dust) was estimated to be 1.38 ± 0.15, suggesting that this type of dust was moderately hygroscopic. (The uncertainty reported is a fit uncertainty; it is possible that the derived GF(85%) for type I dust is somewhat overestimated from limitations of linear extrapolation. Further details are provided in the supporting information (Figure S8).) In contrast, the GF(85%) for Type II dust was 1.01 ± 0.14, indicating that it is overall much less hygroscopic than Type I dust. This suggests that the CaO component of dust is less hygroscopic than the SiO_2 and Al_2O_3 components, as CaO made up a larger fraction of the Type II dust. These results are consistent with the prior findings by *Lack et al*. [2009], who estimated an average GF(85%) of ~1.25 for 2.1 μm dust particles during the same major Saharan dust event. For comparison, *Pan et al*. [2009] reported a mean $f_{sca}(80\%)$ of 1.20 during a dust episode in Beijing, and *Carrico et al*. [2003] determined $f_{sca}(82.5\%)$ values of 1.18 and 1.39 for PM_{10} and PM_1 particles, respectively, observed during a dust storm period on board the R/V *Ron Brown* during ACE-Asia. Also, during ACE-Asia, *Kim et al*. [2006] observed $f_{sca}(85\%)$ as high as 2.00 (±0.27) for PM_{10} dust particles that had originated from the Gobi desert at a ground site in Korea. Our study, together with the previous findings by *Lack et al*. [2009], suggests that the Saharan dust particles are either inherently somewhat hygroscopic or during long-range transport over the ocean can become hygroscopic. Whatever the reason, it is evident that dusts from different sources have different hygroscopicities, hence differently influence the hygroscopic behavior of the bulk aerosols.

4.3.2. Estimation of Supermicron Organics Growth Factor Through Hygroscopicity Closure

Organic aerosol is an important component in the supermicron size range, yet its hygroscopic properties have not been extensively characterized in the ambient atmosphere before. Organics were found to contribute to the supermicron mass to a similar extent as nonsea-salt inorganic ions (TexAQS) or to both nonsea-salt inorganic ions and IOM (CalNex) (Figure 4). In this study, the investigation of hygroscopic growth of supermicron organics during TexAQS was possible through an analysis of hygroscopicity closure since the GF(85%) of IOM was explicitly constrained by observations above, and the GFs of the other inorganic components are also known. The basic idea is that in a hygroscopicity closure study the growth factor of the mixture (GF_{mixed}) can be estimated from the growth factors of individual aerosol components and their volume fraction (ε), using the Zdanovskii-Stokes-Robinson volume-weighted mixing rule [*Zdanovskii*, 1948; *Stokes and Robinson*, 1966; *Gysel et al*., 2007; *Hersey et al*., 2009]:

$$GF_{mixed} = \left(\sum_i \varepsilon_i GF_i^3 \right)^{\frac{1}{3}} \quad (6)$$

In equation (6), GF_{mixed} corresponds to the derived GF values determined from inversion of the $f_{ext}(RH)$ observations. Assuming a constant growth factor for the supermicron organics (GF_{OM}) at 85% RH that equals either 1 or 1.3 (i.e., the range of values determined for the submicron OM) leads to substantial underestimation of the overall supermicron $GF_{mixed}(85\%)$ (Figure S9), suggesting that supermicron organics are largely more hygroscopic than the submicron organics in this study. The absolute values of the bulk-average $GF_{OM}(85\%)$ were determined for each observed GF(85%) by minimizing the root mean square error between the observed $GF_{super}(85\%)$ and calculated $GF_{mixed}(85\%)$. Table 2 lists the individual

Table 2. Parameters (Growth Factor, Density, and Volume Fraction of Each Supermicron Particle Component) and the Associated Uncertainty Used in the Hygroscopicity Closure With Monte Carlo Analysis

		GF(85%)	Density (g cm^{-3})	Volume Fraction[d]
IOM	CaO	Type I: 1.38[a]	3.35	28.8% ± 4.5%
	Al_2O_3	Type II: 1.01 + 13.6%	3.95	
	SiO_2		2.65	
	Fe_2O_3		5.24	
	TiO_2		4.23	
NaCl (SS)		2.05 ± 0.05	2.15	19.5 ± 2.6%
$NaNO_3$		1.65 ± 0.05	1.78	16.6 ± 2.2%
$(NH_4)_2SO_4$		1.5 ± 0.05	1.78	5.2 ± 0.7%
OM		TBD[b]	1.11[c]	30.0% ± 9.9%

[a]For the type I dust, a left-skewed and offset Weibull probability distribution (Figure S11) was adopted to account for the possible overestimate of GF_{IOM}(85%) introduced by the extrapolation of the linear fit of GF_{super}(85%) versus the IOM mass fraction (Figure 6).
[b]To be determined as part of the closure.
[c]The density of organic matter was calculated from the ratio of organic aerosol mass and the difference between the total aerosol volume determined with an APS and the sum of the volumes of the individual inorganic components.
[d]The campaign-average volume fraction and the associated measurement uncertainty for each component. Note that the time-dependent volume fractions associated with each individual GF(85%) measurement are used in the optical closure. The total uncertainty in the volume fraction includes those associated with the total particle volume distribution measurement and the impactor mass measurement of each component.

component GF(85%) and the density used to convert mass fractions into volume fractions for each of the different aerosol components. Based on the ammonium-to-sulfate molar ratio, $(NH_4)_2SO_4$ was assumed to be the main form of supermicron sulfate, and $NaNO_3$ was assumed to be the main form of supermicron nitrate. The temporal variation of the volume fractions of the various supermicron aerosol components is presented in Figure S10. The uncertainty associated with the hygroscopicity closure calculation and the derived GF_{OM} (85%) was systematically assessed through a Monte Carlo analysis. Values for each of the model input parameters (Table 2), including the overall supermicron GF(85%), were randomly sampled from probability distributions that were assumed to be independent and normally distributed about each parameter's mean value (GFs were constrained to be >1), with the exception of the GF(85%) for the type I dust. For the type I dust, a left-skewed and offset Weibull probability distribution (Figure S11) was used to account for the possible overestimate of GF_{IOM}(85%) introduced by the extrapolation of the linear fit of GF_{super}(85%) versus the IOM mass fraction (Figure 6). GF_{OM}(85%) values were derived 20,000 times to determine a frequency distribution of GF_{OM}(85%) values for each observed overall GF(85%). Approximately 35% of the model inputs were unrealistic (e.g., gave a negative organic volume fraction) and therefore were discarded.

Figure 7 shows a time series of the inferred supermicron GF_{OM}(85%) from the hygroscopicity closure with the calculation uncertainty obtained from the Monte Carlo analysis. The campaign-average GF_{OM}(85%) was 1.59 (±0.19), suggesting the appreciable contribution of water uptake from organics for supermicron particles. Despite the relatively large uncertainty associated with the estimated GF_{OM}(85%), variations in the GF_{OM} (85%) during the course of the TexAQS study appear to be linked to the air mass source regions. Consideration of HYSPLIT back trajectories associated with different periods indicate that lower GF_{OM}(85%) values, most frequently encountered near the end of the campaign in September, were mainly associated with continental U.S./polluted air mass origins. Comparably higher GF_{OM}(85%) values, typically sampled earlier during the cruise, were linked to air masses that originated from the ocean (Gulf of Mexico or Atlantic Ocean) and/or long-range transport from Africa with likely atmospheric processing. For example, the supermicron GF_{OM}(85%) was estimated to be 1.26, 1.35, and 1.18 on 18 August, 30 August, and 7 September, respectively, when the air mass trajectories were clearly from the continental U.S. (Figure 7). These values are in the range of the submicron GF_{OM}(85%) (~1.0-1.3) determined in this study (Figure 5) and reported elsewhere [*Randles et al.*, 2004; *Hersey et al.*, 2009; *Zamora et al.*, 2011; *Gantt and Meskhidze*, 2013], suggesting that supermicron OM from continental sources may be chemically similar to submicron OM. In contrast, marine or long-range supermicron OM on average had a substantially higher GF_{OM}(85%), which could imply a different chemical composition associated with the different particle origins. It is possible that some marine primary organic aerosols (e.g., fungi and bacteria) make up a large fraction of the supermicron OM mass in the marine boundary layer, and they likely have different hygroscopic behaviors from the organic

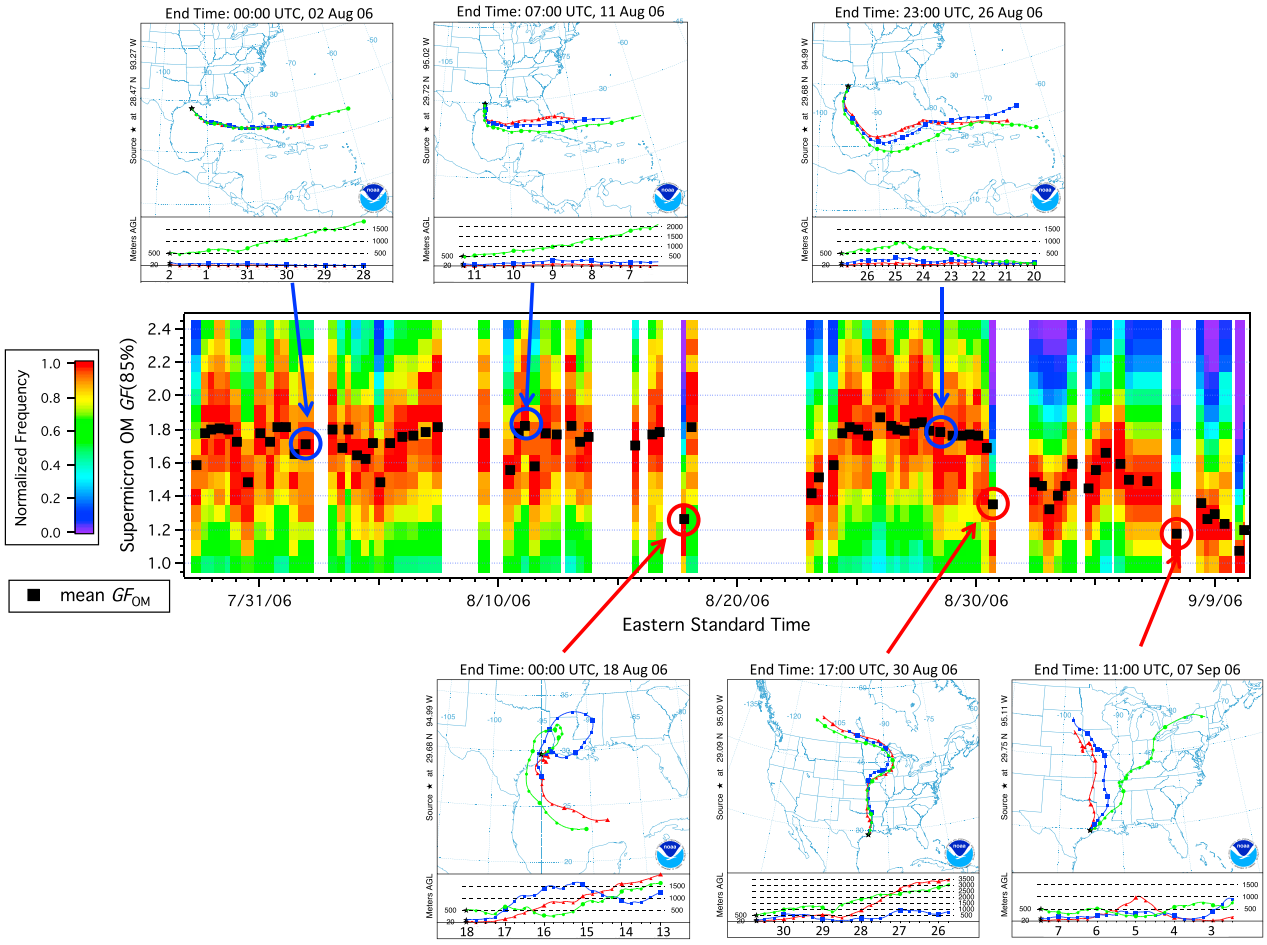

Figure 7. The central panel shows a time series of the frequency distribution of the inferred supermicron GF_{OM}(85%) from hygroscopicity closure calculation with 20,000 run Monte Carlo simulation. The color represents the normalized frequency (between 0 and 1) of the supermicron GF_{OM}(85%) ranged from 1.0 to 2.5 with 0.1 increment. The black squares represent the mean supermicron GF_{OM}(85%). The surrounding panels show 5 day (7 day in one case) HYSPLIT back trajectories that indicate air mass origin for selected impactor sampling periods during the cruise. HYSPLIT results were obtained from http://ready.arl.noaa.gov/HYSPLIT.php. The horizontal dashed lines indicate altitude, and are spaced by 500 m. The line colors indicate the end-point altitude of the air mass: surface (red), 20 m (blue), 500 m (green).

compounds formed from gas-particle conversion [*Hawkins and Russell*, 2010]. However, since no further chemical information regarding the nature of the supermicron OM is available for this study, we cannot comment on the type of organic compounds or functional groups that may lead to the highly hygroscopic behaviors of the overall supermicron organics. In addition, given the uncertainty associated with the inversion approach, the possibility that the mean GF_{OM}(85%) was biased high cannot be completely ruled out.

5. Conclusion

Subsaturated hygroscopic properties of both submicron and supermicron aerosols in the remote and coastal marine boundary layers during three research cruises, TexAQS-GoMACCS 2006, ICEALOT 2008, and CalNex 2010, were investigated using an optical approach. The impact of water uptake on particle light extinction, f_{ext}(RH), was quantified with a cavity ring-down aerosol extinction spectrometer (CRD-AES) making extinction measurement at 532 nm under dry (<30%) and elevated (i.e., 75% and 85%) RHs. An optically weighted bulk growth factor (GF) at 85% RH for both submicron and supermicron aerosols was retrieved from the f_{ext}(85%) measurement based on Mie theory calculations. The derived GF(85%) was proved to be a more robust measure for hygroscopic growth than f_{ext}(85%), which can be confounded by changes in particle dry size distribution. The link between aerosol hygroscopic growth and chemical composition was examined for both size ranges. Broadly consistent with previous studies, a negative correlation was found between submicron GF(85%) (GF_{sub}) and the submicron organic mass fraction (mf_{OM}), although the slopes of the

linear regression fit between the two showed moderate sensitivity to the mass fraction of dust and sea salt. For supermicron aerosols, $GF_{super}(85\%)$ was reasonably well correlated with the supermicron sea-salt mass fraction. Hygroscopic behaviors of other supermicron components (i.e., dust and organics) were studied using TexAQS 2006 as a case. Two types of dust with distinct hygroscopic properties were identified. The dust aerosols that originated from the Saharan desert were moderately hygroscopic, with an average GF of 1.38 ± 0.15, whereas the dust from continental (possibly industrial) sources was nearly hydrophobic, with an average GF of 1.01 ± 0.14. With the GFs for the IOM and other inorganic components constrained, the bulk GF(85%) for supermicron organics (GF_{OM}) was determined with a hygroscopicity closure calculation based on volume-weighted mixing rule. Uncertainties in the derived $GF_{OM}(85\%)$ were estimated through a Monte Carlo analysis that accounted for uncertainties in each of the closure input parameters. Minimization of the difference between observed and predicted GFs for the mixture yielded a campaign-average $GF_{OM}(85\%)$ of 1.59 (±0.19) for the supermicron organics, suggesting the important role that the supermicron OM plays in influencing the overall aerosol water uptake. The supermicron organics that originated from the marine environment were found to have much higher $GF_{OM}(85\%)$ values than those that originated from continental U.S./industrial sources, suggesting that marine organic aerosols likely have distinct chemical composition. The continental supermicron organics had hygroscopicity similar to the submicron organics.

This study provides an addition to the literature of marine aerosol hygroscopic properties and observational constraints for climate models, with new insights on the hygroscopic properties of supermicron aerosol components, of which our knowledge are still very limited. The relatively large water uptake potential of supermicron marine aerosols underlines their importance in determining the aerosol radiative forcing, yet the lack of understanding on their chemical composition, sources, and hygroscopic and optical behaviors poses great challenge in accurately quantifying their climate impact.

Acknowledgments

This analysis was supported by the NOAA Climate Program Office (NA09OAR4310124) and the U.S. Environmental Protection Agency under a STAR research assistance agreement (RD834558). This work has not been formally reviewed by any of the funding agencies. The views expressed in this document are solely those of the authors, and the funding agencies do not endorse any products or commercial services mentioned in this publication. The three cruises were primarily supported by NOAA with additional support from the California Air Resources Board (CalNex) and the Texas Air Quality Study (TexAQS). The authors would like to acknowledge Derek Coffman and Kristen Schulz at NOAA PMEL for the collection of the size distribution and impactor data, respectively. We also thank the crews of NOAA R/V *Ronald H. Brown*, WHOI R/V *Knorr*, and the WHOI R/V *Atlantis* who made this study possible.

References

Allan, J. D., J. L. Jimenez, P. I. Williams, M. R. Alfarra, K. N. Bower, J. T. Jayne, H. Coe, and D. R. Worsnop (2003), Quantitative sampling using an Aerodyne aerosol mass spectrometer 1. Techniques of data interpretation and error analysis, *J. Geophys. Res.*, *108*(D3), 4090, doi:10.1029/2002JD002358.

Bates, T. S., D. J. Coffman, D. S. Covert, and P. K. Quinn (2002), Regional marine boundary layer aerosol size distributions in the Indian, Atlantic, and Pacific Oceans: A comparison of INDOEX measurements with ACE-1, ACE-2, and Aerosols99, *J. Geophys. Res.*, *107*(D19), 8026, doi:10.1029/2001JD001174.

Bates, T. S., et al. (2004), Marine boundary layer dust and pollution transport associated with the passage of a frontal system over eastern Asia, *J. Geophys. Res.*, *109*, D19S19, doi:10.1029/2003JD004094.

Bates, T. S., et al. (2008), Boundary layer aerosol chemistry during TexAQS/GoMACCS 2006: Insights into aerosol sources and transformation processes, *J. Geophys. Res.*, *113*, D00F01, doi:10.1029/2008JD010023.

Berner, A., C. Lürzer, F. Pohl, O. Preining, and P. Wagner (1979), The size distribution of the urban aerosol in Vienna, *Sci. Total Environ.*, *13*, 245–261, doi:10.1016/0048-9697(79)90105-0.

Bohren, C. F., and D. R. Huffman (1983), *Absorption and Scattering of Light by Small Particles*, 530 pp., John Wiley, New York.

Cappa, C. D., D. L. Che, S. H. Kessler, J. H. Kroll, and K. R. Wilson (2011), Variations in organic aerosol optical and hygroscopic properties upon heterogeneous OH oxidation, *J. Geophys. Res.*, *116*, D15204, doi:10.1029/2011JD015918.

Carrico, C. M., P. Kus, M. J. Rood, P. K. Quinn, and T. S. Bates (2003), Mixtures of pollution, dust, sea salt, and volcanic aerosol during ACE-Asia: Radiative properties as a function of relative humidity, *J. Geophys. Res.*, *108*(D23), 8650, doi:10.1029/2003JD003405.

Cerully, K. M., et al. (2011), *Atmos. Chem. Phys.*, *11*, 12,369–12,386, doi:10.5194/acp-11-12369-2011.

Draxler, R. R., and G. D. Rolph (2013), HYSPLIT (Hybrid Single-Particle Lagrangian Integrated Trajectory) model access via NOAA ARL READY website. [Available at http://www.arl.noaa.gov/HYSPLIT.php.] NOAA Air Resources Laboratory, College Park, Md.

Duplissy, J., et al. (2011), Relating hygroscopicity and composition of organic aerosol particulate matter, *Atmos. Chem. Phys.*, *11*, 1155–1165, doi:10.5194/acp-11-1155-2011.

Flores, J. M., R. Z. Bar-Or, N. Bluvshtein, A. Abo-Riziq, A. Kostinski, S. Borrmann, I. Koren, I. Koren, and Y. Rudich (2012), Absorbing aerosols at high relative humidity: Linking hygroscopic growth to optical properties, *Atmos. Chem. Phys.*, *12*, 5511–5521, doi:10.5194/acp-12-5511-2012.

Formenti, P., W. Elbert, W. Maenhaut, J. Haywood, and M. O. Andreae (2003), Chemical composition of mineral dust aerosol during the Saharan Dust Experiment (SHADE) airborne campaign in the Cape Verde region, September 2000, *J. Geophys. Res.*, *108*(D18), 8576, doi:10.1029/2002JD002648.

Frossard, A. A., P. M. Shaw, L. M. Russell, J. H. Kroll, M. R. Canagaratna, D. R. Worsnop, P. K. Quinn, and T. S. Bates (2011), Springtime Arctic haze contributions of submicron organic particles from European and Asian combustion sources, *J. Geophys. Res.*, *116*, D05205, doi:10.1029/2010JD015178.

Gantt, B., and N. Meskhidze (2013), The physical and chemical characteristics of marine primary organic aerosol: A review, *Atmos. Chem. Phys.*, *13*, 3979–3996, doi:10.5194/acp-13-3979-2013.

Gassó, S., et al. (2000), Influence of humidity on the aerosol scattering coefficient and its effect on the upwelling radiance during ACE-2, *Tellus B*, *52*, 546–567, doi:10.1034/j.1600-0889.2000.00055.x.

Ghan, S. J., X. Liu, R. C. Easter, R. Zaveri, P. J. Rasch, and J.-H. Yoon (2012), Toward a minimal representation of aerosols in climate models: Comparative decomposition of aerosol direct, semidirect, and indirect radiative forcing, *J. Clim.*, *25*, 6461–6476.

Gysel, M., J. Crosier, D. O. Topping, J. D. Whitehead, K. N. Bower, M. J. Cubison, P. I. Williams, M. J. Flynn, G. B. McFiggans, and H. Coe (2007), Closure study between chemical composition and hygroscopic growth of aerosol particles during TORCH2, *Atmos. Chem. Phys.*, *7*, 6131–6144.

Hawkins, L. N., and L. M. Russell (2010), Polysaccharides, proteins, and phytoplankton fragments: Four chemically distinct types of marine primary organic aerosol classified by single particle spectromicroscopy, *Adv. Meteorol.*, *2010*, doi:10.1155/2010/612132.

Hegg, D. A., D. S. Covert, K. K. Crahan, H. H. Jonsson, and Y. Liu (2006), Measurements of aerosol size-resolved hygroscopicity at sub and supermicron sizes, *Geophys. Res. Lett.*, *33*, L21808, doi:10.1029/2006GL026747.

Hegg, D. A., D. S. Covert, and H. H. Jonsson (2008), Measurements of size-resolved hygroscopicity in the California coastal zone, *Atmos. Chem. Phys.*, *8*, 7193–7203.

Hersey, S. P., A. Sorooshian, S. M. Murphy, R. C. Flagan, and J. H. Seinfeld (2009), Aerosol hygroscopicity in the marine atmosphere: A closure study using high-time-resolution, multiple-RH DASH-SP and size-resolved C-ToF-AMS data, *Atmos. Chem. Phys.*, *9*, 2543–2554.

Hersey, S. P., et al. (2013), Composition and hygroscopicity of the Los Angeles Aerosol: CalNex, *J. Geophys. Res. Atmos.*, *118*, 3016–3036, doi:10.1002/jgrd.50307.

Hitzenberger, R., A. Berner, U. Dusek, and R. Alabashi (1997), Humidity-dependent growth of size-segregated aerosol samples, *Aerosol Sci. Technol.*, *27*, 116–130, doi:10.1080/02786829708965461.

Intergovernmental Panel on Climate Change (2007), *IPCC: Intergovernmental Panel on Climate Change, Fourth Assessment Record*, Cambridge Univ. Press, Cambridge, U. K., and New York.

Jayne, J. T., D. C. Leard, X. F. Zhang, P. Davidovits, K. A. Smith, C. E. Kolb, and D. R. Worsnop (2000), Development of an aerosol mass spectrometer for size and composition analysis of submicron particles, *Aerosol Sci. Technol.*, *33*, 49–70, doi:10.1080/027868200410840.

Kim, J., S. C. Yoon, A. Jefferson, and S. W. Kim (2006), Aerosol hygroscopic properties during Asian dust, pollution, and biomass burning episodes at Gosan, Korea in April 2001, *Atmos. Environ.*, *40*, 1550–1560, doi:10.1016/j.atmosenv.2005.10.044.

Kinne, S., et al. (2003), Monthly averages of aerosol properties: A global comparison among models, satellite data, and AERONET ground data, *J. Geophys. Res.*, *108*(D20), 4634, doi:10.1029/2001JD001253.

Köhler, H. (1921), Zur Kondensation des Wassers in der Atmosphäre, *Meteorol. Z.*, *38*, 168–171.

Köhler, H. (1936), The nucleus in and the growth of hygroscopic droplets, *Trans. Faraday Soc.*, *32*, 1152–1161.

Lack, D. A., et al. (2009), Relative humidity dependence of light absorption by mineral dust after long-range atmospheric transport from the Sahara, *Geophys. Res. Lett.*, *36*, L24805, doi:10.1029/2009GL041002.

Lambe, A. T., et al. (2013), Relationship between oxidation level and optical properties of secondary organic aerosol, *Environ. Sci. Technol.*, *47*, 6349–6357, doi:10.1021/es401043j.

Langridge, J. M., M. S. Richardson, D. Lack, D. Law, and D. M. Murphy (2011), Aircraft instrument for comprehensive characterization of aerosol optical properties. Part I: Wavelength-dependent optical extinction and its relative humidity dependence measured using cavity ringdown spectroscopy, *Aerosol Sci. Technol.*, *45*, 1305–1318, doi:10.1080/02786826.2011.592745.

Liu, B. Y. H., D. Y. H. Pui, K. T. Whitby, D. B. Kittelson, Y. Kousaka, and R. L. McKenzie (1978), Aerosol mobility chromatograph—New detector for sulfuric-acid aerosols, *Atmos. Environ.*, *12*, 99–104, doi:10.1016/0004-6981(78)90192-0.

Malm, W. C., and D. E. Day (2001), Estimates of aerosol species scattering characteristics as a function of relative humidity, *Atmos. Environ.*, *35*, 2845–2860.

Malm, W. C., and S. M. Kreidenweis (1997), The effects of models of aerosol hygroscopicity on the apportionment of extinction, *Atmos. Environ.*, *31*, 1965–1976, doi:10.1016/s1352-2310(96)00355-x.

Malm, W. C., J. F. Sisler, D. Huffman, R. A. Eldred, and T. A. Cahill (1994), Spatial and seasonal trends in particle concentration and optical extinction in the United States, *J. Geophys. Res.*, *99*, 1347–1370, doi:10.1029/93JD02916.

Malm, W. C., D. E. Day, S. M. Kreidenweis, J. L. Collett, and T. Lee (2003), Humidity-dependent optical properties of fine particles during the Big Bend Regional Aerosol and Visibility Observational Study, *J. Geophys. Res.*, *108*(D9), 4279, doi:10.1029/2002JD002998.

Massoli, P., T. S. Bates, P. K. Quinn, D. A. Lack, T. Baynard, B. M. Lerner, S. C. Tucker, J. Brioude, A. Stohl, and E. J. Williams (2009), Aerosol optical and hygroscopic properties during TexAQS-GoMACCS 2006 and their impact on aerosol direct radiative forcing, *J. Geophys. Res.*, *114*, D00F07, doi:10.1029/2008JD011604.

McInnes, L., M. Bergin, J. Ogren, and S. Schwartz (1998), Apportionment of light scattering and hygroscopic growth to aerosol composition, *Geophys. Res Lett.*, *25*, 513–516, doi:10.1029/98GL00127.

National Institute for Occupational Safety and Health (1996), NIOSH elemental carbon (diesel particulate): Method 5040, in *NIOSH Manual of Analytical Methods*, Cincinnati, OH, National Institute for Occupational Safety and Health.

Pan, X. L., P. Yan, J. Tang, J. Z. Ma, Z. F. Wang, A. Gbaguidi, and Y. L. Sun (2009), Observational study of influence of aerosol hygroscopic growth on scattering coefficient over rural area near Beijing mega-city, *Atmos. Chem. Phys.*, *9*, 7519–7530.

Prather, K. A., et al. (2013), Bringing the ocean into the laboratory to probe the chemical complexity of sea spray aerosol, *Proc. Natl. Acad. Sci. U.S.A.*, *110*, 7550–7555, doi:10.1073/pnas.1300262110.

Quinn, P. K., and T. S. Bates (2003), North American, Asian, and Indian haze: Similar regional impacts on climate?, *Geophys. Res. Lett.*, *30*(11), 1555, doi:10.1029/2003GL016934.

Quinn, P. K., et al. (2005), Impact of particulate organic matter on the relative humidity dependence of light scattering: A simplified parameterization, *Geophys. Res. Lett.*, *32*, L22809, doi:10.1029/2005GL024322.

Quinn, P. K., et al. (2006), Impacts of sources and aging on submicrometer aerosol properties in the marine boundary layer across the Gulf of Maine, *J. Geophys. Res.*, *111*, D23S36, doi:10.1029/2006JD007582.

Rader, D. J., and P. H. McMurry (1986), Application of the tandem differential mobility analyzer to studies of droplet growth or evaporation, *J. Aerosol Sci.*, *17*, 771–787, doi:10.1016/0021-8502(86)90031-5.

Randles, C. A., L. M. Russell, and V. Ramaswamy (2004), Hygroscopic and optical properties of organic sea salt aerosol and consequences for climate forcing, *Geophys. Res. Lett.*, *31*, L16108, doi:10.1029/2004GL020628.

Ryerson, T. B., et al. (2013), The 2010 California Research at the Nexus of Air Quality and Climate Change (CalNex) field study, *J. Geophys. Res. Atmos.*, *118*, 5830–5866, doi:10.1002/jgrd.50331.

Sorooshian, A., S. Hersey, F. J. Brechtel, A. Corless, R. C. Flagan, and J. H. Seinfeld (2008), Rapid, size-resolved aerosol hygroscopic growth measurements: Differential aerosol sizing and hygroscopicity spectrometer probe (DASH-SP), *Aerosol Sci. Technol.*, *42*, 445–464, doi:10.1080/02786820802178506.

Stock, M., Y. F. Cheng, W. Birmili, A. Massling, B. Wehner, T. Muller, S. Leinert, N. Kalivitis, N. Mihalopoulos, and A. Wiedensohler (2011), Hygroscopic properties of atmospheric aerosol particles over the Eastern Mediterranean: Implications for regional direct radiative forcing under clean and polluted conditions, *Atmos. Chem. Phys.*, *11*, 4251–4271, doi:10.5194/acp-11-4251-2011.

Stokes, R. H., and R. A. Robinson (1966), Interactions in aqueous nonelectrolyte solutions. I. Solute-solvent equilibria, *J. Phys. Chem.*, *70*, 2126–2130.

Turpin, B. J., and H. Lim (2001), Species contribution to PM2.5 concentrations: Revisiting common assumptions for estimating organic mass, *Aerosol Sci. Technol.*, *35*, 602–610, doi:10.1080/02786820152051454.

Virkkula, A., R. Van Dingenen, F. Raes, and J. Hjorth (1999), Hygroscopic properties of aerosol formed by oxidation of limonene, α-pinene, and β-pinene, *J. Geophys. Res.*, *104*, 3569–3579, doi:10.1029/1998JD100017.

Wang, W., M. J. Rood, C. M. Carrico, D. S. Covert, P. K. Quinn, and T. S. Bates (2007), Aerosol optical properties along the northeast coast of North America during the New England Air Quality Study—Intercontinental Transport and Chemical Transformation 2004 campaign and the influence of aerosol composition, *J. Geophys. Res.*, *112*, D10S23, doi:10.1029/2006JD007579.

Wu, Z. J., et al. (2013), Relating particle hygroscopicity and CCN activity to chemical composition during the HCCT-2010 field campaign, *Atmos. Chem. Phys.*, *13*, 7983–7996, doi:10.5194/acp-13-7983-2013.

Zamora, I. R., A. Tabazadeh, D. M. Golden, and M. Z. Jacobson (2011), Hygroscopic growth of common organic aerosol solutes, including humic substances, as derived from water activity measurements, *J. Geophys. Res.*, *116*, D23207, doi:10.1029/2011JD016067.

Zdanovskii, A. (1948), New methods for calculating solubilities of electrolytes in multicomponent systems, *Zhur. Fiz. Khim.*, *22*, 1475–1485.

Zhang, X., B. J. Turpin, P. H. McMurry, S. V. Hering, and M. R. Stolzenburg (1994), Mie theory evaluation of species contributions to 1990 wintertime visibility reduction in the Grand Canyon, *J. Air Waste Manag. Assoc.*, *44*, 153–162.

Ziemba, L. D., et al. (2013), Airborne observations of aerosol extinction by in situ and remote-sensing techniques: Evaluation of particle hygroscopicity, *Geophys. Res. Lett.*, *40*, 1–6, doi:10.1029/2012GL054428.